Linear stability analysis of nonisothermal glass fiber drawing

Julien Philippi*
TIPs, Université Libre de Bruxelles, C.P. 165/67, Avenue F. D. Roosevelt 50, 1050 Brussels, Belgium

Mathias Bechert
Forschungszentrum Jülich GmbH, Helmholtz Institute Erlangen-Nürnberg for Renewable Energy (IEK-11), Fürther Straße 248, 90429 Nuremberg, Germany

Quentin Chouffart and Christophe Waucquez
3B–The Fibreglass Company, Rue de Charneux 59, B-4651 Battice, Belgium

Benoit Scheid
TIPs, Université Libre de Bruxelles, C.P. 165/67, Avenue F. D. Roosevelt 50, 1050 Brussels, Belgium

(Received 10 November 2020; accepted 25 March 2022; published 15 April 2022)

The draw resonance effect appears in fiber drawing processes when the draw ratio, defined as the ratio between the take-up and the inlet velocities, exceeds a critical value. In many cases, inertia, gravity, and surface tension cannot be neglected, and a model combining all these effects is necessary in order to correctly describe the physics of the phenomenon. Additionally, it is also known that cooling can have a highly stabilizing effect on the draw resonance instability. However, a detailed analysis encompassing the effect of inertia, gravity, surface tension, and temperature is still lacking. Due to a destabilizing effect induced by geometry in the heat equation, we first show that the maximum critical draw ratio for fiber drawing can be two orders of magnitude lower than the one for the film casting problem when the heat transfer coefficient is assumed constant. By introducing a scaling making the fiber aspect ratio an independent parameter, we next show that the high value of the critical draw ratio encountered in industrial applications could be rationalized only if we consider that the heat transfer coefficient is not constant but depends on both the velocity and the cross-section area of the fiber. Within this framework, we show how the practical stability window is affected by the five control parameters: the draw ratio, the fiber aspect ratio, the inlet temperature, the convective heat transfer coefficient, and the stiffness of the non-homogeneous ambient temperature. We finally discuss the influence of radiative heat transfer on the stability.

DOI: 10.1103/PhysRevFluids.7.043901

I. INTRODUCTION

Thermal drawing processes are involved in a large range of applications as diverse as the manufacture of glass [1,2] and polymer fibers [3–6], optical fibers [7,8], or more recently multimaterial fibers with advanced functionalities [9–12]. We note that filamentary structures can also be produced naturally during volcanic eruptions. Indeed, magma fragmentation can lead to filaments formation which form as they cool down the so-called Pele's hairs [13]. We focus in this work on a setup consisting of a nozzle of cylindrical shape from which the molten material is extruded. The falling

*julien.philippi@ulb.ac.be

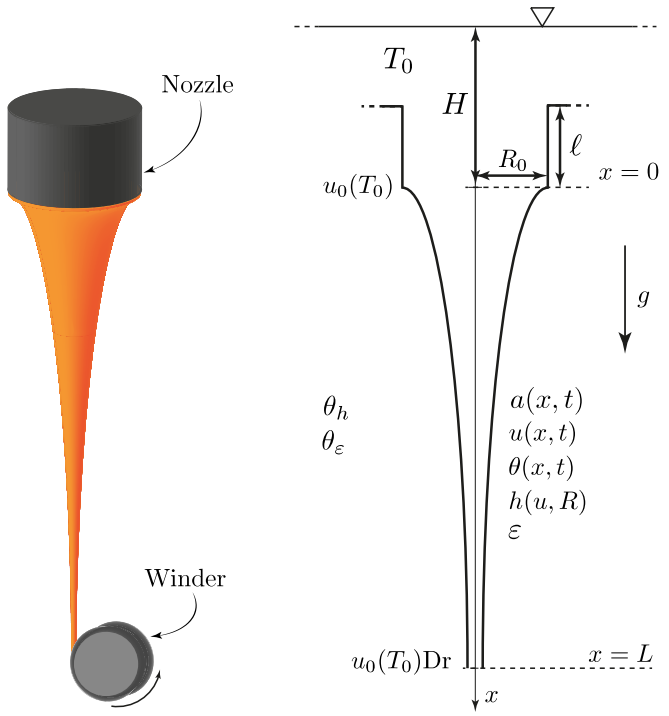

FIG. 1. Left: Sketch of the fiber drawing process. Right: One-dimensional nonisothermal fiber model.

liquid filament is then pulled by a winder in order to considerably reduce the cross-section area of the resulting fiber, as depicted in Fig. 1. The final diameter is controlled by the draw ratio, defined as the ratio of the velocity at the winder to the velocity at the nozzle.

Among all the possible industrial applications, there are some examples where it is possible to take advantage of an hydrodynamical instability. The Rayleigh-Plateau instability, for instance, can be controlled and exploited in order to produce particles by multimaterial in-fiber emulsification [14]. Nevertheless instability phenomena occurring during fiber drawing processes are in general not acceptable as they will modify the expected fiber shape and eventually lead to rupture and process failure [15]. Such an inconvenience is encountered when the draw ratio exceeds a critical value and then triggers the so-called draw resonance instability. The latter results in oscillations of fiber diameter and flow velocity around the fiber centerline. A very basic explanation of the instability mechanism could be given with an argument of continuity. An increase (respectively a decrease) of fiber tension at the outlet induces a feed-back mechanism at the inlet and produces a decrease (respectively an increase) of the diameter at the nozzle exit. This diameter variation is traveling downstream and leads to force reduction (respectively augmentation) as it reaches the outlet. As suggested by Hyun [16] and Kim *et al.* [17], this oscillating behavior which characterizes the draw resonance instability can be seen as a traveling wave phenomenon. More details about the mechanism of the instability can be found in [18,19].

The critical draw ratio is influenced by many physical parameters, and its sensitivity regarding to inertia, gravity, surface tension, and heat transfer has been studied extensively in the past. However, most of these effects have been treated independently in the literature. The pioneering theoretical works studying this problem by means of a linear stability analysis are based on a one-dimensional, purely viscous, and isothermal model [20–22]. In this case the critical draw ratio for draw resonance to occur is 20.218. Shah and Pearson [23] proposed a generalization of the existing models [20,21] by considering separately the effects of inertia, gravity, and surface tension on the stability of

both isothermal and nonisothermal fiber drawing processes. It appears that inertia, gravity, and cooling have a stabilizing effect while surface tension destabilizes the system. They have also shown that there exists a threshold value of the heat transfer coefficient beyond which the system is unconditionally stable, while Scheid *et al.* have later shown, even though only for films, that approaching the limit of infinite heat transfer coefficient should have a destabilizing effect [18].

Although the destabilizing effect of surface tension was evidenced for decades [23,24], it appears that this physical quantity has been widely considered negligible for the study of the draw resonance instability. Recently the combined influence of inertia, gravity, and surface tension on draw resonance in the isothermal case had been investigated [19] utilizing a linear stability analysis. The resulting stability maps reveal that the destabilizing influence of surface tension can overcome the stabilization induced by inertia and gravity and eventually lead to unconditional instability even for low values of the surface tension parameter.

Most of the studies considering nonisothermal fiber drawing focus merely on convective heat transfer. However, Hyunh and Tanner [25] showed that radiation is the dominant transfer in the first few millimeters below the nozzle. Myers [26] have evidenced the existence of regimes where radiation have a stabilizing effect by assuming that radiative exchange is the main form of heat transfer and by considering that viscous extensional stress is the only contribution in the momentum equation.

To the best of our knowledge, despite the wide number of studies dedicated to fiber drawing in the literature, no study has simultaneously investigated the effects of inertia, gravity, and surface tension in the nonisothermal case. As shown by Bechert and Scheid [19], surface tension can have a significant destabilizing effect on fiber drawing processes, so that it cannot be neglected, as is commonly assumed. Therefore it is still necessary to determine the mechanism which overcomes the destabilizing effect of surface tension and permits one to reach a production draw ratio of the order of 10^4 as encountered in industrial applications.

We revisit and generalize in this study the seminal works of Shah and Pearson [23] in a more exhaustive way by proposing a nonisothermal one-dimensional model encompassing inertia, gravity, and surface tension as well as convective and radiative heat transfer. The scaling is adapted to handle this multiparametric problem by isolating the control parameters relevant to practical applications, namely, the inlet temperature and the fiber aspect ratio, in a real setup. A linear stability analysis is then performed in order to produce neutral stability curves by numerical continuation in a way which permits to explore the full parameter space. The influence of the viscosity law, ambient temperature decrease, and varying heat transfer coefficient on the stability are first determined using the purely viscous model. The stability behavior for the full model is then investigated with an emphasis on the effect of the aspect ratio, inlet temperature, and stiffness of the decreasing ambient temperature along the fiber. Each of the parameters used in this study has been chosen in a range relevant to glass fiber manufacturing. The paper ends with a discussion and conclusions.

II. NONISOTHERMAL MODEL

As the nozzle radius is usually much smaller than the drawing length, the slender fiber approximation is applicable. Therefore we follow the classical approach used in the literature [20,23,27] and base our study on a one-dimensional model. We consider the extensional flow of velocity $u(x, t)$ along the x axis of a viscous liquid filament of length L drawn at its bottom by a winder, referred to as the outlet, at a constant velocity u_L. The filament is fed at its top by molten glass at temperature θ_0 through a cylindrical nozzle of radius R_0 and height ℓ at velocity $u(0, t) = u_0(\theta_0)$ as sketched in Fig. 1. The exit point of the nozzle is referred to as the inlet. With the velocity at the outlet u_L being the quantity used to set the final radius of the fiber, the draw ratio, defined as

$$\mathrm{Dr} = \frac{u_L}{u_0}, \tag{1}$$

is the natural control parameter of the problem. The filament of cross-section area $a(x, t)$ is assumed axisymmetric.

With molten glass being the only material considered in this study, we assume that the liquid is Newtonian and that its temperature-dependent dynamic viscosity $\eta(\theta)$ is given by the Vogel-Fulcher-Tamman (VFT) law, which is widely used in the field of glass processing and given by [28]

$$\log \eta(\theta) = \log \eta_\infty + \frac{B}{\theta - \theta_c}, \tag{2}$$

where $\theta = \theta(x, t)$ denotes the cross-section-averaged temperature of the fiber and η_∞, B, and θ_c are three constants which depend on the glass composition. In all generality this framework can be applied to any kind of Newtonian molten materials. The evolution of the temperature field is governed by both convective and radiative heat transfer. The heat transfer coefficient h is not constant. Indeed, it appears that it depends explicitly on the velocity and on the cross-section area of the fiber, following previous studies [1,29]. As we consider the stability of a single fiber in the present study, which excludes chaotic air motion occurring in a fiber bundle, the air flow induced by the process is expected to be laminar. In this regime, the most commonly used model in the literature [23,30] providing an explicit relation $h = h(a, u)$ has been proposed by Kase and Matsuo [29]. These authors measured experimentally the heat transfer coefficient of a heated wire in air flow and obtained for the particular case of a flow parallel to the fiber a relation of the following form:

$$h(a, u) = \frac{0.42\pi^{1/3} k_a}{\nu^{1/3}} \left(\frac{u}{a}\right)^{\frac{1}{3}}, \tag{3}$$

where k_a and ν are respectively the thermal conductivity and kinematic viscosity of air. As mentioned above, in many practical applications, fiber drawing can involve a bundle of several thousand fibers. In such cases, the air flow can be chaotic, and an explicit modeling for the heat transfer coefficient can be challenging. Molten glass is here considered as an opaque medium, and internal radiation is neglected [2]. Therefore radiative heat transfer is modeled through a constant effective emissivity of glass fiber surface ε. The convective and radiative heat transfer are parametrized by a reference temperature, θ_h and θ_ε, respectively. Indeed, in a manufacturing process, thousands of fibers are produced simultaneously, and it is not possible to define the ambient temperature as the constant temperature far from the fiber. Therefore it is necessary to define the external temperature through process-dependent approximations leading to θ_h and θ_ε. These estimations correspond to experimental or numerical measurements obtained in the region where each of the contributions is dominant. As radiative and convective exchanges are dominant close to the nozzle and along the fiber, respectively, we impose two different reference temperatures, as encountered in [2,31].

By adopting the same scaling as in [19], the free-fall velocity $\sqrt{gL}$, with gravitational acceleration g, is used as reference velocity. This choice permits us to set the velocity scale directly from the chosen length scale. All variables are nondimensionalized according to the following transformations:

$$\begin{aligned} &x \to Lx, \quad a \to R_0^2 a, \quad t \to \sqrt{\frac{L}{g}}\, t, \\ &u \to \sqrt{gL}\, u, \quad \eta \to \eta_0 \eta, \quad h \to h_0\, h, \\ &\varepsilon \to \varepsilon_0\, \varepsilon, \quad (\theta, \theta_h, \theta_\varepsilon) \to \theta_c + \Delta\theta\, (\theta, \theta_h, \theta_\varepsilon), \end{aligned} \tag{4}$$

where t is the time variable, $\eta_0 = \eta(\theta_0)$, $h_0 = 0.42\pi^{1/3} k_a (gL)^{1/6} (\nu R_0^2)^{-1/3}$ is the convective heat transfer coefficient in $x = 0$, ε_0 is a typical average emissivity along the fiber near the nozzle [2,31], and $\Delta\theta = \theta_0 - \theta_c$. The resulting dimensionless parameters are defined by the following

TABLE I. Dimensional and dimensionless parameters used in the present study. Parameters that are varied in this study are printed in bold.

Dimensional	Value	Dimensionless	Value
$\boldsymbol{L}$ [m]	$\mathbf{6 \times 10^{-2} - 1.8}$	$\boldsymbol{\Lambda}$	$\mathbf{100 - 4000}$
$\boldsymbol{\theta_0}$ [K]	$\mathbf{1543.15 - 1603.15}$	$\boldsymbol{F^*}$	$\mathbf{10^{-3} - 3 \times 10^{-3}}$
$\boldsymbol{h_0}$ [W/(m^2 K)]	$\mathbf{2.805 \times 10^{-3} - 2805}$	$\mathbf{St^*}$	$\mathbf{10^{-8} - 10^{-2}}$
ε_0	0.4	St_r^*	5.8×10^{-5}
γ [N/m]	0.39	S^*	22.4
B [°C]	5262.4	B^*	5.86
H [m]	0.35	θ_c^*	0.45
R_0 [m]	6×10^{-4}	q	10.4
ℓ [m]	4.2×10^{-3}	k	1–30
η_∞ [Pa s]	$10^{-4.075}$	θ_{h_∞}	0.22
θ_c [°C]	402.3	$\theta_{\varepsilon_\infty}$	-0.22
ρ [kg/m^3]	2470		
c_p [J/(kg K)]	1480		

expressions:

$$Q = \frac{u_0}{\sqrt{gL}}, \quad F = \frac{\rho\sqrt{gL^3}}{\eta_0}, \quad S \equiv \left(\frac{\lambda_c}{\sqrt{2R_0L}}\right)^2 = \frac{\gamma}{2\rho g R_0 L},$$
$$\mathrm{St} = \frac{h_0}{\rho c_p R_0}\sqrt{\frac{L}{g}}, \quad \text{and} \quad \mathrm{St}_r = \frac{\varepsilon_0\sigma\,\Delta\theta^3}{\rho c_p R_0}\sqrt{\frac{L}{g}}, \tag{5}$$

where Q, F, S, St, and St_r are respectively the dimensionless inlet velocity, fluidity, surface tension parameter, and the convective and radiative Stanton numbers. A discussion is given in Appendix A to explain how the Stanton number can be constructed on both the Biot and the Péclet numbers, sometimes used in other works [18,30,32,33]. Parameter S compares the capillary length $\lambda_c = \sqrt{\gamma/(\rho g)}$ to the geometric mean of the fiber dimensions, while the Stanton numbers compare the convective and respectively the radiative heat transfer, to the energy advected by the flow; σ is the Stefan-Boltzmann constant, and ρ, γ, and c_p denote density, surface tension, and specific heat capacity of the molten glass, respectively (see Table I). Due to a weak dependence on temperature, each of these three last physical parameters is assumed to be constant in this study. As it could be difficult to properly define the length scale L in industrial applications because of the complexity of the fiber path involving several winders, it is more convenient to consider it as a control parameter of the problem. Hence by introducing the aspect ratio of the fiber $\Lambda = L/R_0$, we propose a set of dimensionless parameters which do not involve the drawing length L:

$$Q^* \equiv \sqrt{\Lambda}\,Q = \frac{u_0}{\sqrt{gR_0}}, \quad F^* \equiv \frac{F}{\Lambda^{\frac{3}{2}}} = \frac{\rho\sqrt{gR_0^3}}{\eta_0}, \quad S^* \equiv \Lambda\,S = \left(\frac{\lambda_c}{\sqrt{2R_0^2}}\right)^2 = \frac{\gamma}{2\rho g R_0^2}, \tag{6}$$

$$\mathrm{St}^* \equiv \frac{\mathrm{St}}{\sqrt{\Lambda}} = \frac{h_0}{\rho c_p\sqrt{gR_0}}, \quad \text{and} \quad \mathrm{St}_r^* \equiv \frac{\mathrm{St}_r}{\sqrt{\Lambda}} = \frac{\varepsilon_0\sigma\,\Delta\theta^3}{\rho c_p\sqrt{gR_0}}. \tag{7}$$

Consequently each of these numbers permits us to control individually an experimentally accessible quantity. More precisely Q^*, F^*, S^*, St^*, and St_r^* respectively, control $u_0(\theta_0)$, $\eta_0(\theta_0)$, γ, h_0, and ε_0. The gauge of the heat transfer coefficient, using (3) at the inlet, becomes $h_0 = 0.42\pi^{1/3}k_a\nu^{-1/3}R_0^{-1/2}(g\Lambda)^{1/6}$. In this configuration, it appears that the temperature at the inlet θ_0 is the main control parameter of the problem as it fixes the value of u_0 and η_0, thus Q^* and F^*. As

mentioned above S^* will be kept constant in the following. Unless specified otherwise, all quantities in the rest of the paper are dimensionless.

In all this study we assume, as in practical cases, that the flow of molten glass through the cylindrical nozzle is a Poiseuille flow driven by an hydrostatic pressure difference. Therefore the velocity at the inlet is not a control parameter and is rather given by $u_0(\theta_0) = \rho g H R_0^2/[8\ell\eta_0(\theta_0)]$ where H is the height of molten glass above the nozzle. Hence the dimensionless inlet velocity becomes $Q^* = (H/8\ell)\,F^*$. More generally it is possible to obtain such a linear relation between Q^* and F^* for any geometry of the nozzle,

$$Q^* = qF^*, \tag{8}$$

where q is a shape factor which permits to account for a specific geometry of the nozzle. Considering the characteristic dimensions of nozzle geometries and molten glass height which could be found in industrial applications, we set $q = H/8\ell = 10.4$ for the shape factor. Consequently the dimensionless inlet velocity Q^* is not an independent parameter when the molten liquid is injected by a fixed hydrostatic pressure difference.

Although cooling induced by convective heat transfer has a clear stabilizing effect [22,23], it has been shown for both film casting [18] and fiber drawing [34] processes that a nonmonotonic behavior of the neutral stability occurs when increasing the Stanton number from the advection-dominated to the heat transfer-dominated regime, which denote the low and high Stanton number regimes respectively. The latter occurs for film casting [18] when $\mathrm{St}^{\mathrm{film}} \approx \Lambda\,\mathrm{St}^*/Q^* \gtrsim 1$, i.e., when $\mathrm{St}^* \gtrsim Q^*/\Lambda$ in the present scaling. In this regime, cooling may be destabilizing when the Stanton number is increased. The same phenomenon has also been evidenced for radiative heat transfer [35,36]. In practical applications, the ambient temperature in the vicinity of the fiber is nonhomogeneous (see discussion in Appendix B). Here we follow the same approach as used by Willien *et al.* [36] by assuming that the ambient temperature θ_h considered for convective heat transfer follows an exponential decay along the fiber,

$$\theta_h = \theta_{h_\infty} + (1 - \theta_{h_\infty})\,\mathrm{e}^{-kx}, \tag{9}$$

where k is a stiffness parameter and θ_{h_∞} is the dimensionless far field temperature associated to convective heat transfer. As an additional justification of (9), since the fiber temperature should take the ambient one in the infinite Stanton number limit, this ambient temperature could not reasonably be constant, unless leading to irregular solutions arising due to the incompatibility with imposing the boundary condition $\theta(0,t) = 1$. Finally, we impose a constant radiative temperature $\theta_\varepsilon = \theta_{\varepsilon_\infty}$ with $\theta_{\varepsilon_\infty}$ the associated dimensionless far field temperature.

We further hypothesize that the temperature profile is assumed uniform along the radial coordinate of the fiber. Indeed, as shown by Scheid *et al.* [18] for film casting, the influence of the temperature profile across the film thickness on the stability of the system is weak. Additionally, the second-order heat diffusion effect in the longitudinal direction is also neglected for the same reason, as shown for fiber drawing by Gupta *et al.* [30]. Under these assumptions, the governing system of equations for the nonisothermal fiber drawing can be rewritten by combining, using the scaling presented above, the cross-section averaged continuity and momentum equations proposed in Bechert and Scheid [19], with the time-dependent version of the leading-order energy equation written in Taroni *et al.* [32]:

$$\partial_t a + \partial_x(au) = 0, \tag{10a}$$

$$\mathrm{F}^*\Lambda^{\frac{3}{2}} a\left(\partial_t u + u\partial_x u - 1 - \frac{\mathrm{S}^*}{\Lambda}\frac{\partial_x a}{a^{\frac{3}{2}}}\right) = \partial_x(3\eta a\partial_x u), \tag{10b}$$

$$\begin{aligned}\partial_t\theta + u\partial_x\theta = -2\sqrt{\frac{\Lambda}{a}}\{&\mathrm{St}^*\,h(a,u)(\theta - \theta_h)\\ &+\mathrm{St}_r^*\left[(\theta_c^* + \theta)^4 - (\theta_c^* + \theta_\varepsilon)^4\right]\},\end{aligned} \tag{10c}$$

with $\theta_c^* = \frac{\theta_c}{\Delta\theta}$. This system is closed through the dimensionless VFT law, which couples the momentum equation (10b) and the energy equation (10c):

$$\eta(\theta) = 10^{B^*\left(\frac{1}{\theta}-1\right)}, \tag{11}$$

where $B^* = \frac{B}{\Delta\theta}$, as well as with the dimensionless Kase and Matsuo law:

$$h(a,u) = \left(\frac{u}{a}\right)^{\frac{1}{3}}. \tag{12}$$

The associated boundary conditions are given at any time t by

$$a(0,t) = 1, \quad u(0,t) = \frac{q\mathrm{F}^*}{\sqrt{\Lambda}}, \quad u(1,t) = \frac{q\mathrm{F}^*}{\sqrt{\Lambda}}\,\mathrm{Dr}, \quad \theta(0,t) = 1. \tag{13}$$

In the case of $\mathrm{St}^* \to 0$ and $\mathrm{St}_r^* \to 0$ we recover the isothermal problem in [19], but with additional flexibility of independently varying the dimensionless drawing length Λ. The parameter values used in this study are displayed in Table I and have been chosen according to practical applications involving molten glass [2,31]. The parameters St_r^*, B^*, and θ_c^* have small variations regarding the range of inlet temperature θ_0 considered in this study. For the sake of simplicity, we impose their value on the one corresponding to $\theta_0 = 1573.15$ K as these variations have a minor influence on the stability curves (data not shown). The ranges of values for the fiber length L and heat transfer coefficient h_0 proposed in this paper are broader than the ones found in industrial applications in order to widely explore the influence of these control parameters.

III. STABILITY ANALYSIS

We study here the stability of the system of equations (10a), (10b), and (10c) by introducing perturbations of amplitude much smaller than unity around the steady state. The latter corresponds to the solution of the governing equations obtained when the time derivative is set to zero. Even though it is not strictly necessary, we also expand for convenience the constitutive equation (11) in the same way. We thus introduce the following expansions:

$$a(x,t) = a_s(x)(1 + A(x)\mathrm{e}^{\lambda t}), \tag{14a}$$

$$u(x,t) = u_s(x)(1 + U(x)\mathrm{e}^{\lambda t}), \tag{14b}$$

$$\theta(x,t) = \theta_s(x)(1 + \Theta(x)\mathrm{e}^{\lambda t}), \tag{14c}$$

$$\eta(x,t) = \eta_s(x)(1 + \Gamma(x)\mathrm{e}^{\lambda t}), \tag{14d}$$

where the subscript s identifies the steady state. A, U, Θ, and Γ represent the complex spatial perturbations, and $\lambda = \lambda_R + i\,\lambda_I$ is the complex eigenvalue. The complex conjugate terms are omitted for the sake of readability. λ_R and λ_I respectively represent the growth rate of the instability and the pulsation. Within this framework the steady state is determined by the following equations:

$$a_s' = -\frac{a_s u_s'}{u_s}, \tag{15a}$$

$$u_s'' = -\frac{a_s' u_s'}{a_s} + \frac{\mathrm{F}^* \Lambda^{\frac{3}{2}}}{3\eta_s}\left(u_s' u_s - 1 - \frac{\mathrm{S}^*}{\Lambda}\frac{a_s'}{a_s^{3/2}}\right) - \frac{\eta_s' u_s'}{\eta_s}, \tag{15b}$$

$$\theta_s' = -\frac{2}{u_s}\sqrt{\frac{\Lambda}{a_s}}\left\{\mathrm{St}^*\, h(a_s,u_s)\,(\theta_s - \theta_h) + \mathrm{St}_r^*\left[(\theta_c^* + \theta_s)^4 - (\theta_c^* + \theta_\varepsilon)^4\right]\right\}, \tag{15c}$$

$$\eta_s = 10^{B^*\left(\frac{1}{\theta_s}-1\right)}, \tag{15d}$$

where the prime corresponds to the derivative with respect to x. By introducing the expansions (14) into Eqs. (10) and (11), and by linearizing the resulting equations for small perturbations, we obtain the following perturbation equations:

$$A' = -\left(\frac{\lambda}{u_s}A + U'\right), \tag{16a}$$

$$U'' = \frac{\lambda u_s'}{u_s^2}A + \frac{\mathrm{F}^*\Lambda^{\frac{3}{2}}}{3\eta_s}\left[\left(\frac{1}{u_s} + \lambda + u_s'\right)U + u_s U' + \frac{\mathrm{S}^*}{\Lambda\sqrt{a_s}u_s^2}\left[\left(\lambda - \frac{u_s'}{2}\right)A - u_s'(U+\Gamma) + u_s U'\right]\right.$$
$$\left. + \left(\frac{1}{u_s} - u_s'\right)\Gamma\right] - \frac{u_s'}{u_s}\Gamma' - \frac{\eta_s'}{\eta_s}U', \tag{16b}$$

$$\Theta' = -\frac{\lambda}{u_s}\Theta - \frac{2\,\mathrm{St}^*}{u_s\theta_s}\sqrt{\frac{\Lambda}{a_s}}\left(h(a_s,u_s)\theta_h\Theta - (\theta_s - \theta_h)\left\{h(a_s,u_s)\left(U + \frac{A}{2}\right)\right.\right.$$
$$\left.\left. - [a_s\partial_{a_s}h(a_s,u_s)A + u_s\partial_{u_s}h(a_s,u_s)U]\right\}\right)$$
$$- \frac{2\,\mathrm{St}_r^*}{u_s\theta_s}\sqrt{\frac{\Lambda}{a_s}}\left\{4\,\theta_s(\theta_c^* + \theta_s)^3\Theta - \left[(\theta_c^* + \theta_s)^4 - (\theta_c^* + \theta_\varepsilon)^4\right]\left(U + \frac{A}{2} + \Theta\right)\right\}, \tag{16c}$$

$$\Gamma = -\log(10)B^*\frac{\Theta}{\theta_s}. \tag{16d}$$

The steady state satisfies the boundary conditions (13), while the perturbations have to vanish where the variables are fixed according to these boundary conditions,

$$A(0) = U(0) = \Theta(0) = 0 \quad \text{and} \quad U(1) = 0. \tag{17}$$

With the eigenvalue problem (16) being linear and homogeneous, the amplitude of the solutions is arbitrary. We thus choose to fix the perturbation A of the fiber cross-section area at the outlet to unity, i.e., $A(1) = 1$. This choice has no influence on the eigenvalue spectrum and thus on the calculated stability [23].

The stability of the system regarding thermal effects is studied by solving the system of ODEs (15) and (16). For very high values of the critical draw ratio, the stationary cross-section area a_s decreases down to extremely small values that can make problematic the numerical resolution of some terms in (15) and (16) where it appears at the denominator. A simple way to circumvent this problem is to make use of the mass conservation equation to substitute in these terms the stationary cross-section variable by

$$a_s = \frac{Q^*}{u_s\sqrt{\Lambda}}. \tag{18}$$

We consider here the first mode of the instability, which corresponds to the eigenvalue with the highest real part. The value of the critical draw ratio Dr_c is deduced by tracking the solution for which $\lambda_R = 0$. The neutral stability curves giving the evolution of Dr_c as a function of the Stanton number St^* is obtained by using a numerical continuation method with the open-source code AUTO-07p [37] as described in previous works [18,19,38,39]. The purely viscous isothermal solution, i.e., the solution derived for $F^* = \mathrm{St}^* = 0$, which can be obtained analytically [40,41], is used as a starting point.

IV. PURELY VISCOUS NONISOTHERMAL MODEL ($F^* = 0$)

It is well known that cooling has a stabilizing effect on the draw resonance instability in the advection-dominated regime [18,23,30]. However, to the best of our knowledge the mechanism

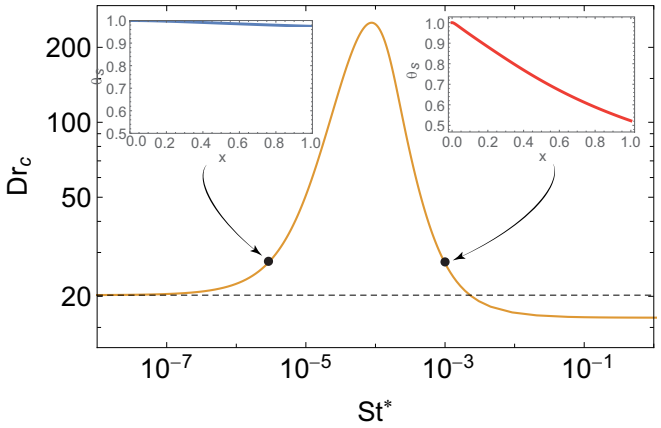

FIG. 2. Critical draw ratio as a function of the Stanton number St^* for the purely viscous model with convective heat transfer only ($\mathrm{St}_r^* = 0$) and a VFT viscosity law. The curve is computed for a constant heat transfer coefficient, an aspect ratio $\Lambda = 10^3$, an inlet temperature $\theta_0 = 1573.15$ K, $\theta_{h_\infty} = 0.22$, and $k = 1$. The inset represent the steady temperature $\theta_s(x)$ for $\mathrm{St}^* = 2.5 \times 10^{-6}$ (blue curve) and 10^{-3} (red curve) and characterizes the advection-dominated and heat transfer-dominated regimes, respectively.

responsible for the stability of fiber drawing processes for draw ratio up to 10^4 is not well understood yet. Such a high critical draw ratio has already been observed for film casting in the study of Scheid *et al.* [18]. However, the same observation does not stand for fiber drawing as shown in Fig. 2, which represents the neutral stability curve for the purely viscous case with a VFT viscosity law, a constant heat transfer coefficient, and a stiffness parameter $k = 1$. By transposing the exact same model than Scheid *et al.* [18] to the fiber drawing case, we can see that the maximum critical draw ratio is two orders of magnitude lower (see Appendix C). This large difference arises from a destabilizing effect due to geometry characterized by the $a^{-1/2}$ dependance in the right-hand side of the energy equation (10c) (instead of a^{-1} for film casting). As detailed in Appendix D, it also appears that another choice of the viscosity law cannot explain the dramatic stabilization observed in industrial applications. In this section we determine the influence of the ambient temperature through the stiffness parameter k and the heat transfer coefficient on the stability of the system. For this purpose, we here use the purely viscous model, i.e., neglecting inertia, gravity, and surface tension, all addressed in Sec. V, and exclude radiative heat transfer ($\mathrm{St}_r^* = 0$), which will be addressed in Sec. V D. The purely viscous model is obtained by setting $F^* = 0$ in (10b) with the following boundary conditions:

$$u(0,t) = \frac{Q^*}{\sqrt{\Lambda}},\ u(1,t) = \frac{Q^*}{\sqrt{\Lambda}}\,\mathrm{Dr}, \tag{19}$$

where Q^* has been fixed to $Q^*(\theta_0 = 1573.15\,\mathrm{K}) \approx 1.93 \times 10^{-2}$.

A. Influence of the non-homogeneous ambient temperature

The choice of the spatially dependent ambient temperature has a strong influence on the stability of the system. Indeed, as shown in Fig. 3(a), the value of the maximum critical draw ratio rises significantly by increasing the value of the stiffness parameter k. At some point, this maximum becomes even higher than the limit of the domain covered in this study, say, $\mathrm{Dr} \leqslant 10^5$, which encompasses the domain for practical applications. Nonetheless the maximum value of Dr_c should remain finite. We then compute two portions of the neutral stability curves leading to a central stability window when $k > 5$. The left portion rises dramatically with the Stanton number up to critical draw ratio as high as 10^5 and is in the advection-dominated regime, while the right one,

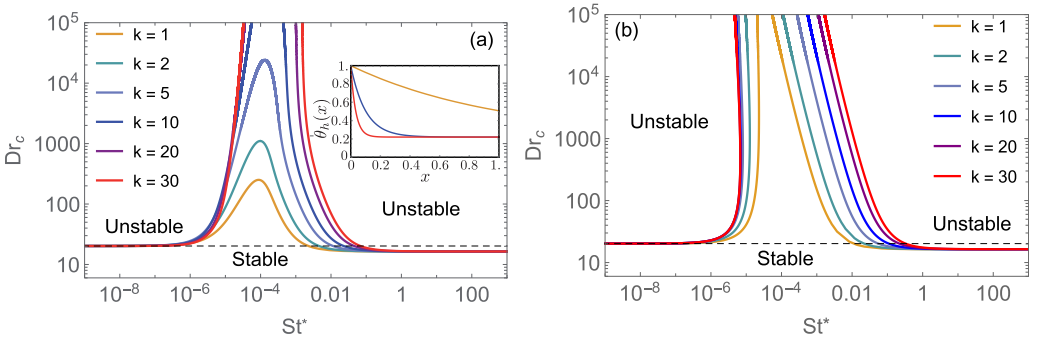

FIG. 3. Neutral stability curves for the purely viscous model with convective heat transfer only ($\mathrm{St}_r^* = 0$) and a VFT viscosity law. Each curve is computed for a fiber of aspect ratio $\Lambda = 10^3$, an inlet temperature $\theta_0 = 1573.15$ K and $\theta_{h_\infty} = 0.22$. The black dashed line represents the classical value $\mathrm{Dr}_c = 20.218$ encountered in the isothermal case. (a) Influence of the non-homogeneous ambient temperature: critical draw ratio as a function of the Stanton number St^* with $k = 1, 2, 5, 10, 20$, and 30 for a constant heat transfer coefficient. The inset represents the ambient temperature $\theta_h(x)$ for $k = 1, 10$, and 30. (b) Influence of the heat transfer coefficient governing law: critical draw ratio as a function of the Stanton number St^* with $k = 1, 2, 5, 10, 20$, and 30 for a heat transfer coefficient following the Kase and Matsuo model (12).

located in the heat transfer-dominated regime, strongly decreases with St^* and finally reaches the limit critical draw ratio corresponding to the case $k = 1$. The width of the stability window increases with k as the right portion shifts toward the large St^* values, while the left portion does not evolve anymore. The production draw ratio being of the order of 10^4 in practical applications, we can see that as soon as $k > 5$ the system admits an operating window compatible with such values, i.e. for $\mathrm{Dr}_c > 10^4$. In order to obtain a wide enough stable operating window for $\mathrm{Dr} \sim 10^4$, and unless specified otherwise, we take $k = 30$ as a reference value in the following. Larger values have been found to give similar results (not shown) while bringing numerical difficulties due to the extremely steep temperature gradient it implies near the inlet.

B. Influence of nonconstant heat transfer coefficient

The neutral stability curves evidencing the effect of a nonconstant heat transfer coefficient are plotted in Fig. 3(b). It appears that cooling has a highly stabilizing effect when the heat transfer coefficient follows the Kase and Matsuo model, whatever the value of the stiffness parameter. Indeed, just as previously with the largest values of k, the maximum critical draw ratio rises dramatically. Although this value should remain finite, the latter exceeds the limit of the domain covered in this study, say, $\mathrm{Dr} \leqslant 10^5$, even for the case $k = 1$. Then, regarding the maximum critical draw ratio, the choice of the stiffness parameter value is less important than the heat transfer coefficient varying along the fiber. Nevertheless, the stability window resulting from this behavior becomes wider as k increases. We also note that for any value of the stiffness parameter the left portion admits a turning point. This important stabilization can be understood by considering the fact that with $a_s u_s$ being constant, the heat transfer coefficient corresponding to the stationary solutions follows the relation $h(a_s, u_s) \propto a_s^{-2/3}$. Then as the cross-section area decreases along the fiber, the heat transfer coefficient increases in turn. With the system being in the advection-dominated regime, an increasing heat transfer towards the outlet has a stabilizing effect on the system according to previous studies on film casting [18]. It thus demonstrates the crucial importance of accounting for a nonlinear heat transfer coefficient in thermal fiber drawing.

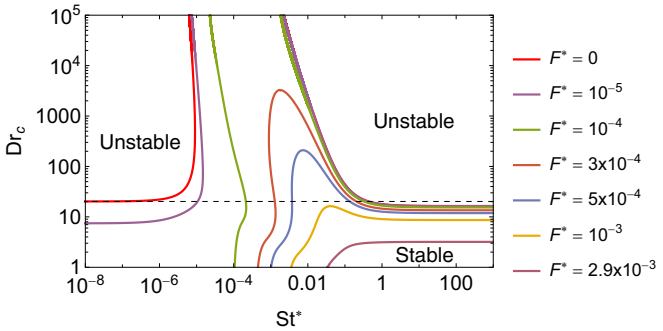

FIG. 4. Influence of the fluidity F^*: critical draw ratio as a function of the Stanton number St^* computed for various values of the fluidity F^*, with an aspect ratio $\Lambda = 1000$ and a stiffness parameter $k = 30$. The dimensionless inlet velocity is fixed to its value corresponding to $\theta_0 = 1603.15$ K. The black dashed line represents the classical value $\mathrm{Dr}_c = 20.218$ encountered in the purely viscous isothermal case.

V. FULL NONISOTHERMAL MODEL ($F^* > 0$)

From now on, inertia, gravity, and surface tension are taken into account, and we assume that viscosity and heat transfer coefficient follow a VFT law and the Kase and Matsuo model, respectively.

A. Preliminary study for the full model: Influence of the fluidity F^*

It is now well established that capillary effect through radial curvature has a dramatic destabilizing effect regarding draw resonance instability [19]. In order to characterize the effect of the surface tension term (proportional to F^*S^* in the momentum equation) in the nonisothermal framework, we first show the influence of the fluidity alone on the stability. Thus we represent in Fig. 4 the neutral stability curves obtained for different values of F^* with a dimensionless inlet velocity fixed to $Q^*(\theta_0 = 1603.15\ \mathrm{K})$ and an aspect ratio $\Lambda = 1000$. It appears that a dramatic destabilization of the system occurs as the fluidity increases. Indeed, as seen with the purely viscous case, the maximum critical draw ratio is not attainable when the fluidity is low. However, the surface tension has an important destabilizing effect as soon as $F^* = O(10^{-4})$. It appears that the system admits a regime of unconditional instability as the critical draw ratio can reach unity while its maximum value (if any) decreases at a very strong rate when the fluidity increases. Ultimately the maximum value of Dr_c becomes even lower than 10 when $F^* \approx 3 \times 10^{-3}$. We also note that the Stanton number necessary to attain a stable region increases with F^*, and likewise for the maximum critical draw ratio. Finally we can see that the surface tension effect is also of higher importance in the nonisothermal framework and that cooling is not enough to stabilize the system at any condition. The following sections will be dedicated to the determination of the conditions leading to an important stabilization of the cooling.

B. Influence of the aspect ratio Λ

The neutral stability curves for the full model determined for different values of the fiber aspect ratio are represented in Fig. 5 for a fixed inlet temperature. As long as $\Lambda < 100$, the neutral stability curves admit a maximum out of the domain for practical applications. Similarly to the purely viscous case, we compute two portions of the neutral stability curves leading to a central stability window with critical draw ratio up to 10^5. The left portion admits a turning point at $\mathrm{Dr}_c \sim 10$, similarly to the purely viscous case (see Sec. IV B). Hence above this bifurcation point, critical draw ratio increases as the heat transfer decreases. This behavior results from a nonintuitive phenomenon. Indeed, for a fixed value of the Stanton number it is possible to reach a stable region from an unstable one

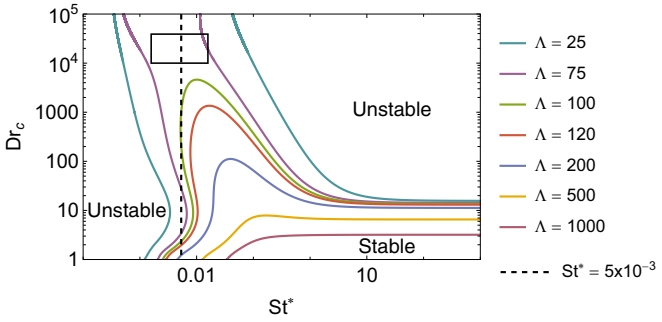

FIG. 5. Influence of the fiber aspect ratio: critical draw ratio as a function of the Stanton number St^* computed for fibers of different values of the aspect ratio Λ, with an inlet temperature $\theta_0 = 1603.15$ K and a stiffness parameter $k = 30$. The range of industrial applications is represented by a black box centered around the realistic Stanton number $\mathrm{St}^* = 5 \times 10^{-3}$.

by simply raising the draw ratio. Such a behavior had already been observed both experimentally and numerically for glass fiber drawing [31]. We also note that the critical draw ratio does not converge to the value of 20.218 corresponding to the purely viscous case as $\mathrm{St}^* \to 0$ due to surface tension effects, as shown in [19]. As in the purely viscous case the right portion goes to $\mathrm{Dr}_c \sim 16$ as $\mathrm{St}^* \to \infty$.

It appears that increasing the control parameter Λ when the inlet temperature is fixed destabilizes the system independently of the value of θ_0. First, the size of the stability window decreases as Λ increases, and for $\Lambda \gtrsim 100$, the maximum critical draw ratio decreases dramatically with Λ. Eventually the latter becomes of order unity. The black box drawn in Fig. 5 represents a typical range of values of the couple $(\mathrm{Dr}, \mathrm{St}^*)$ encountered in industrial applications. The latter is in a region of strong variability of the critical draw ratio with Λ. We can see that a small variation of the heat transfer coefficient is enough to change the stability of the system for many values of the fiber aspect ratio as exemplified in Fig. 5 with the black dashed line $\mathrm{St}^* = 5 \times 10^{-3}$. Therefore, the appropriate determination of the fiber aspect ratio to be imposed in the model is of major interest. Indeed, phase change through a glass transition occurs at some region of the fiber, and its locus obviously determines the correct value of Λ, which remains, in such a framework, an unknown of the problem.

C. Influence of the inlet temperature θ_0 and stiffness parameter k

The influence of the inlet temperature θ_0 on the neutral stability curves for the full model encompassing the effects of inertia, gravity, and surface tension with a purely convective heat transfer is depicted in Fig. 6(a).

We note that for a given value of the aspect ratio, increasing θ_0 has always a destabilizing effect since the stability curves are shifted toward higher values of the heat transfer by conserving their shapes. This behavior is independent of the value of Λ (data not shown). As the inlet temperature controls the fluidity through the viscosity, F^* increases with θ_0. Both inertia and gravity scale with the fluidity, and both have a stabilizing effect. However, the surface tension parameter is particularly high in our problem. Therefore the surface tension term, which is proportional to F^*S^* in the momentum equation (10b), becomes more and more important, and so the system becomes less and less stable in the low Stanton number regime as θ_0 increases.

The influence of the non-homogeneous ambient temperature through the stiffness parameter k on the stability of the system is represented in Fig. 6(b) for a fixed inlet temperature and aspect ratio. Just as in the purely viscous case, we note that the maximum critical draw ratio increases with k and admits a variation of two orders of magnitude between $k = 10$ and $k = 30$. Therefore,

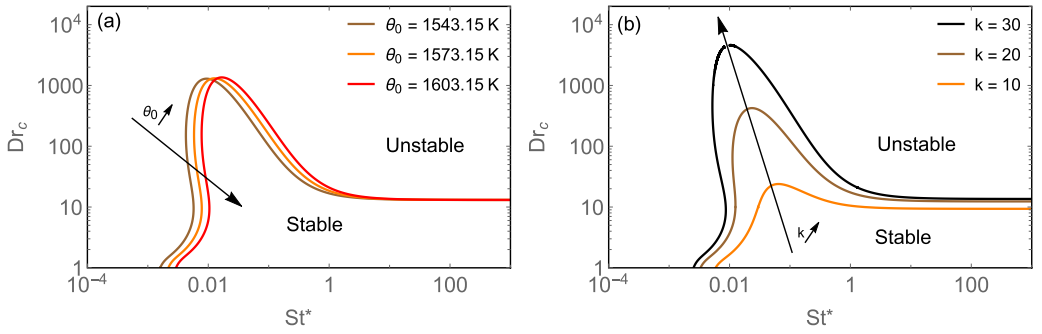

FIG. 6. (a) Influence of the inlet temperature on the stability of the system for the full model with convective heat transfer only ($St_r^* = 0$). Critical draw ratio as a function of the Stanton number St^* computed with $F^* = 1.2 \times 10^{-3}$, 1.9×10^{-3}, and 2.9×10^{-3}, respectively corresponding to inlet temperatures $\theta_0 = 1543.15$, 1573.15, and 1603.15 K. Each curve is obtained for a fiber of aspect ratio $\Lambda = 120$ and a stiffness parameter $k = 30$. (b) Critical draw ratio as a function of the Stanton number St^* computed for stiffness parameter $k = 10$, 20, and 30 with an inlet temperature $\theta_0 = 1603.15$ K and an aspect ratio $\Lambda = 100$.

a precise depiction of the non-homogeneous ambient temperature surrounding the fiber will be of fundamental interest for industrial applications in order to correctly estimate the critical draw ratio. As the stability of the system is very sensitive to the stiffness of the ambient temperature and to the aspect ratio, the temperature of the nozzle θ_0 could be adapted in order to reach a stable region.

D. Influence of the radiative heat transfer

As shown by Hyunh and Tanner [25], heat exchanges by radiation have an important influence on the first few millimeters below the nozzle and have to be taken into account in the boundary conditions. By fixing ε_0 to a realistic value corresponding to industrial applications (see Table I), the radiative Stanton number is determined only by θ_0. The influence of the radiative heat transfer is depicted in Fig. 7. It compares the neutral stability curves for the full model when radiation is taken into account with those obtained in the purely convective limit. We can see here a stabilizing effect of radiation, especially as $St^* \to 0$. More precisely, stability curves do not reach regions of unconditional instability (i.e., $Dr_c < 1$) with radiation, although the critical draw ratio remains low

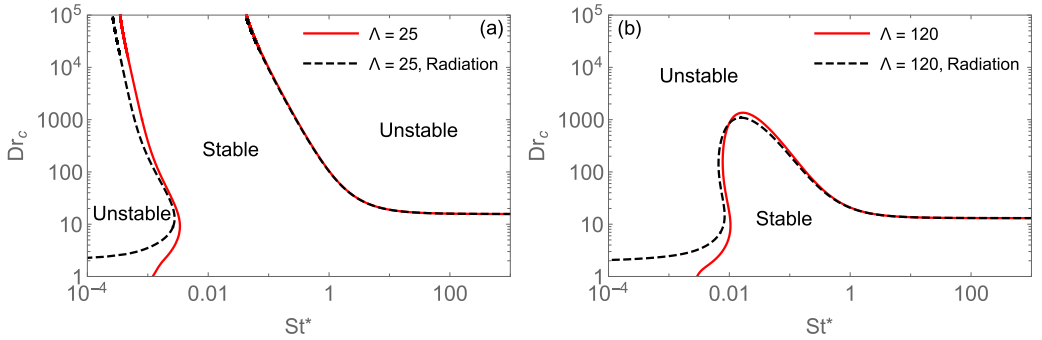

FIG. 7. Influence of radiative heat transfer on the stability of the system. Neutral stability curves for the full model represented in the case of a pure convective heat transfer (continuous line) and convective and radiative heat transfer (dashed line) for $\Lambda = 25$ (a) and 120 (b). Each curve is computed for an inlet temperature $\theta_0 = 1603.15$ K and $k = 30$. The radiative Stanton number is fixed to $St_r^* = 5.8 \times 10^{-5}$. The viscosity and the heat transfer coefficient respectively follow a VFT law and the Kase and Matsuo model.

when the Stanton number becomes very small. Indeed, for any value of Λ, $\mathrm{Dr}_c \approx 2$ in the low Stanton number limit. We also note that the locus of the bifurcation point occurs at a slightly lower value of the Stanton number.

VI. DISCUSSION

The current model we proposed could still be improved in several ways. In many industrial applications, the fluid entering in the system through the nozzle simply flows due to gravity. Therefore an hydrostatic pressure is applied at the inlet, and a coupling between dynamic pressure $p \sim \eta_0 \partial_x u$, induced by the extensional flow and velocity fields has to be considered in order to impose a correct boundary condition. Indeed, by considering that the Poiseuille flow in the nozzle is driven by the pressure difference determined by a static and a dynamic contribution, the calculation of the flow rate leads to the following Robin boundary condition:

$$u(0,t) = \frac{qF^*}{\sqrt{\Lambda}} + \frac{R_0}{8\ell\Lambda}\partial_x u(0,t). \tag{20}$$

As draw resonance instability is a problem which strongly depends on boundary conditions [40], we expect that such a correction will have an important influence on the stability.

Moreover, the temperature reached in our system due to cooling is always sufficiently high to avoid phase change, namely, the glass transition point. However, it has been shown for both Newtonian and non-Newtonian fluids that solidification has an influence on the stability [42–44]. Nevertheless to the best of our knowledge all the physical effects that are relevant in the problem are not taken into account simultaneously in the existing literature. We also note that if the position of the freezing (or glass transition) point is above the winder, the fiber length we have to consider in the system must be modified accordingly. Consequently a full model encompassing phase change has to be developed. A variable fiber length, as proposed here, is an attempt to deal with this issue, and certainly demonstrates the sensitivity of the stability with respect to this parameter.

Finally, we have shown the limitation of our model due to surface tension effects when the drawing is not sufficient. By adding the effect of longitudinal surface tension, the transition from draw resonance to Rayleigh-Plateau instability has also to be investigated.

VII. CONCLUSION

We have investigated in the present study the stability of Newtonian fiber drawing processes with an emphasis on molten glass in the nonisothermal case. Our one-dimensional model generalizes the one proposed by Bechert and Scheid [19], which encompass simultaneously the effects of inertia, gravity, and surface tension by adding the cross-section averaged energy equation for convective and radiative heat transfer. The system is closed through the VFT law, which characterizes the temperature-dependent viscosity. With the length L of the system being not always very well defined, and should depend on the glass transition point, we have chosen to consider it as a control parameter of the problem via the aspect ratio. Therefore we have introduced an alternative scaling involving Λ and based on the one proposed in [19]. Finally the fiber drawing model for molten glass we have proposed is governed by five control parameters: the draw ratio Dr, the inlet temperature θ_0, the Stanton number St^*, the fiber aspect ratio Λ, and the stiffness k of the ambient temperature decay.

By the use of a linear stability analysis we have first shown in the purely viscous regime that the strong stabilization induced by cooling is not related to the law of viscosity we consider but is rather due to the modeling of the heat transfer coefficient of the fiber through the Kase and Matsuo model [29]. Within this framework we obtain a model explaining how it is possible to reach critical draw ratio as high as 10^4, as encountered in industrial applications.

By considering the model including inertia, gravity, and surface tension for convective heat transfer only we evidenced that increasing Λ strongly destabilizes the system. We have also demonstrated

that the stability of the system is very sensitive to non-homogeneous ambient temperature, while a variation of the inlet temperature induces a slight shift of the stability region. These two last parameters can be used to change effectively the critical draw ratio as soon as the heat transfer coefficient is imposed. Therefore the determination of the correct fiber aspect ratio through a model taking into account the phase change appears to be a problem of fundamental interest for future research.

ACKNOWLEDGMENTS

We acknowledge 3B–The Fibreglass Company for supporting this research. B.S. thanks the FRS-FNRS for financial support.

APPENDIX A: ON THE DIMENSIONLESS NUMBERS FOR THE HEAT EQUATION

In general terms, the convective Stanton number is defined as $\mathrm{St} = \mathrm{Bi}\,\Lambda/\mathrm{Pe}$, where $\mathrm{Bi} = h_0 R_0/\lambda$ and $\mathrm{Pe} = \rho c_p R_0\sqrt{gL}/\lambda$ are the Biot and the Péclet number respectively, and λ is the thermal conductivity of the liquid; Bi describes the rate of heat transport from the liquid to the surroundings, while Pe/Λ measures the heat advected in the flow direction. A detailed discussion on the relative order of magnitude of Bi and Pe/Λ could be found in Sec. 2.2 of Scheid *et al.* [18], in particular, the fact that the one-dimensional assumption considered in this paper corresponds to the case of $\mathrm{Bi} \ll 1$, with finite St. Consequently, Bi should appear only as an independent parameter in the case one wants to assess the departure of the transverse temperature profile from the uniform one, as investigated in [18] for film casting and in [32] for fiber drawing. Likewise, Pe/Λ should appear only as an independent parameter in the case one wants to assess the second-order thermal diffusion effects in the longitudinal direction, as investigated in [30] for film casting and in [33] for fiber drawing. Since none of these two effects are considered here, the number of dimensionless parameters for the heat equation can be reduced by one when using the convective Stanton number, complemented by the radiative Stanton number if radiative heat transfer is also considered, as done in the present work.

APPENDIX B: ON THE NONHOMOGENEOUS AMBIENT TEMPERATURE

Realistic modeling of fiber drawing processes requires one to consider a varying ambient temperature along the fiber direction, but at least two different configurations exist. (1) In the manufacture of fibre-optic cables, a centimeter-size cylindrical glass preform is lowered into a furnace. In this context, Taroni *et al.* [32] have considered a Gaussian distribution of the furnace radiative temperature, hotter in the central portion and cooler at the ends. Similarly, they have taken a Gaussian distribution of the ambient temperature, three-fourths smaller than the radiative one. (2) In the manufacture of glass fibers for material composite, as considered in the present work, molten glass is flown through a nozzle and drawn in ambient air. There is no furnace around the fiber, which essentially cools down by convective heat transfer. The ambient air is therefore the hottest at the nozzle and drops rapidly in the flow direction, which can be properly described by an exponential decay function, as used by several authors [18,36] and considered in the present work.

APPENDIX C: COMPARISON WITH FILM CASTING IN THE PURELY VISCOUS CASE

Regarding the governing equations, film casting and fiber drawing differ only in the purely viscous case by the right-hand side of the energy equation. As could be seen in the governing equations written for a constant heat transfer coefficient with our current set of dimensionless parameters, this term is inversely proportional to the film thickness R_{film} for film casting [18], while

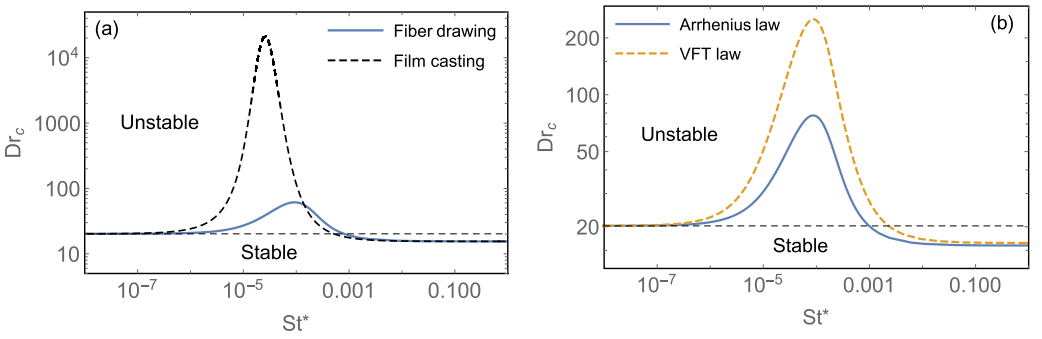

FIG. 8. Neutral stability curves for the purely viscous model with convective heat transfer only ($\mathrm{St}_r^* = 0$) and constant heat transfer coefficient. Each curve is computed for an aspect ratio $\Lambda = \Lambda_{\mathrm{film}} = 10^3$ and an inlet temperature $\theta_0 = 1573.15$ K. (a) Comparison with film casting: critical draw ratio as a function of the Stanton number St^* for film casting (black dashed line) and fiber drawing (blue line) with $\theta_{h_\infty} = 0$ and $k = 1$. The viscosity is given by the Arrhenius law with $\mu = 3$. (b) Influence of the viscosity law for fiber drawing: critical draw ratio as a function of the Stanton number St^* for a temperature-dependent viscosity following an Arrhenius law with $\mu = B^*$ (blue line) and a VFT law (yellow dashed line) with $\theta_{h_\infty} = 0.22$ and $k = 1$. The black dashed line represents the classical value $\mathrm{Dr}_c = 20.218$ encountered in the purely viscous isothermal case.

it is inversely proportional to $\sqrt{a}$ in the present case [see Eq. (10c)]:

$$\partial_t R_{\mathrm{film}} + \partial_x (R_{\mathrm{film}} u) = 0, \tag{C1a}$$

$$\partial_x (\eta R_{\mathrm{film}} \partial_x u) = 0, \tag{C1b}$$

$$\partial_t \theta + u \partial_x \theta = -2 \frac{\sqrt{\Lambda_{\mathrm{film}}}}{R_{\mathrm{film}}} \mathrm{St}^* (\theta - \theta_h), \tag{C1c}$$

where $\Lambda_{\mathrm{film}} = L_{\mathrm{film}}/R_{0,\mathrm{film}}$ is the film aspect ratio with L_{film} the length of the film and $R_{0,\mathrm{film}}$ the film thickness at the inlet. The neutral stability curve obtained from our purely viscous model with a constant heat transfer coefficient is compared to the solution obtained by Scheid *et al.* [18] for film casting in Fig. 8(a). Both cases are computed with the Arrhenius law given by the following relation:

$$\eta \equiv \eta_{\mathrm{A}}(\theta) = e^{\mu\left(\frac{1}{\theta} - 1\right)}, \tag{C2}$$

where μ measures the thermal sensitivity of the viscosity. The ambient temperature is given by $\theta_h = e^{-x}$, which corresponds to the particular case $\theta_{h_\infty} = 0$ and $k = 1$. We note that the neutral stability curves are qualitatively the same. Indeed, heat transfer has a stabilizing effect until the critical draw ratio reaches a maximum and then destabilizes the system as the Stanton number increases further. However, this maximum is two orders of magnitude higher in Dr_c for film casting than for fiber drawing. Additionally, the Stanton number corresponding to the transition from advection-dominated to heat transfer-dominated regime ($\mathrm{St}^* \sim Q^*/\Lambda$) is also higher for fiber drawing. The critical draw ratio converges towards the same value below 20.218 in the large Stanton number limit in both cases, reflecting the scenario of a prescribed, exponentially decreasing temperature [18]. All the computing parameters being the same in each case, it is remarkable that such a small variation of the energy equation leads to a strong variation of the critical draw ratio.

APPENDIX D: INFLUENCE OF THE CONSTITUTIVE LAW IN THE PURELY VISCOUS CASE

The choice of the temperature-viscosity relation obviously depends on the composition of the considered material. The Arrhenius law is widely used in the literature for applications involving

any kind of Newtonian and non-Newtonian fluids [7,12,18,34]. However, it appears that the VFT model is more precise at high temperature for molten glass [2]. The neutral stability curves obtained for a VFT and an Arrhenius viscosity law from the purely viscous model with a constant heat transfer coefficient are represented in Fig. 8(b). We can see that stability curves are not deeply affected by the viscosity law we choose and that stabilization due to cooling is rather weak in this configuration. Indeed, although the critical draw ratio at first starts to increase with heat transfer, it eventually reaches a maximum which corresponds to $\mathrm{Dr}_c \approx 80$ for VFT and $\mathrm{Dr}_c \approx 250$ for Arrhenius law. This maximum occurs for both cases at $\mathrm{St}^* \approx 10^{-4}$. Finally, the critical draw ratio decreases as the Stanton number increases until it reaches a plateau around $\mathrm{Dr}_c = 16$. In this region of the neutral stability curve, the heat transfer becomes very important, and the fiber temperature goes to the limit temperature of the ambient $\theta_h(x)$.

[1] R. Beyreuther and H. Brünig, *Dynamics of Fibre Formation and Processing: Modelling and Application in Fibre and Textile Industry* (Springer, Berlin, Heidelberg, 2007).

[2] Q. Chouffart, P. Simon, and V. E. Terrapon, Numerical and experimental study of the glass flow and heat transfer in the continuous glass fiber drawing process, J. Mater. Process. Technol. **231**, 75 (2016).

[3] J. R. A. Pearson and Y. T. Shah, On the stability of isothermal and nonisothermal fiber spinning of power-law fluids, Ind. Eng. Chem. Fundam. **13**, 134 (1974).

[4] R. J. Fisher and M. M. Denn, A theory of isothermal melt spinning and draw resonance, AIChE J. **22**, 236 (1976).

[5] Y. Demay and J. F. Agassant, An overview of molten polymer drawing instabilities, Int. Polym. Proc. **29**, 128 (2014).

[6] J. Bengtsson, K. Jedvert, T. Köhnke, and H. Theliander, Identifying breach mechanism during air-gap spinning of lignin–cellulose ionic-liquid solutions, J. Appl. Polym. Sci. **136**, 47800 (2019).

[7] P. Gospodinov and A. L. Yarinz, Draw resonance of optical microcapillaries in nonisothermal drawing, Int. J. Multiphase Flow **23**, 967 (1997).

[8] Y. M. Stokes, J. J. Wylie, and M. J. Chen, Coupled fluid and energy flow in fabrication of microstructured optical fibres, J. Fluid Mech. **874**, 548 (2019).

[9] A. F. Abouraddy, M. Bayindir, G. Benoit, S. D. Hart, K. Kuriki, N. Orf, O. Shapira, F. Sorin, B. Temelkuran, and Y. Fink, Towards multimaterial multifunctional fibres that see, hear, sense and communicate, Nat. Mater. **6**, 336 (2007).

[10] S. Egusa, Z. Wang, N. Chocat, Z. M. Ruff, A. M. Stolyarov, D. Shemuly, F. Sorin, P. T. Rakich, J. D. Joannopoulos, and Y. Fink, Multimaterial piezoelectric fibres, Nat. Mater. **9**, 643 (2010).

[11] M. Rein, V. D. Favrod, C. Hou, T. Khudiyev, A. Stolyarov, J. Cox, C.-C. Chung, C. Chhav, M. Ellis, J. Joannopoulos, and Y. Fink, Diode fibres for fabric-based optical communications, Nature (London) **560**, 214 (2018).

[12] A. G. Page, M. Bechert, F. Gallaire, and F. Sorin, Unraveling radial dependency effects in fiber thermal drawing, Appl. Phys. Lett. **115**, 044102 (2019).

[13] E. Villermaux, The formation of filamentary structures from molten silicates: Pele's hair, angel hair, and blown clinker, C. R. Mec. **340**, 555 (2012).

[14] J. J. Kaufman, G. Tao, S. Shabahang, E.-H. Banaei, D. S. Deng, X. Liang, S. G. Johnson, Y. Fink, and A. F. Abouraddy, Structured spheres generated by an in-fibre fluid instability, Nature (London) **487**, 463 (2012).

[15] C. D. Han, R. R. Lamonte, and Y. T. Shah, Studies on melt spinning. III. Flow instabilities in melt spinning: Melt fracture and draw resonance, J. Appl. Polym. Sci. **16**, 3307 (1972).

[16] J. C. Hyun, Theory of draw resonance: Part I. Newtonian fluids, AIChE J. **24**, 418 (1978).

[17] B. M. Kim, J. C. Hyun, J. S. Oh, and S. J. Lee, Kinematic waves in the isothermal melt spinning of Newtonian fluids, AIChE J. **42**, 3164 (1996).

[18] B. Scheid, S. Quiligotti, B. Tran, R. Gy, and H. A. Stone, On the (de)stabilization of draw resonance due to cooling, J. Fluid Mech. **636**, 155 (2009).
[19] M. Bechert and B. Scheid, Combined influence of inertia, gravity, and surface tension on the linear stability of Newtonian fiber spinning, Phys. Rev. Fluids **2**, 113905 (2017).
[20] M. A. Matovich and J. R. A. Pearson, Spinning a molten threadline. steady-state isothermal viscous flows, Ind. Eng. Chem. Fundam. **8**, 512 (1969).
[21] D. Gelder, The stability of fiber drawing processes, Ind. Eng. Chem. Fundam. **10**, 534 (1971).
[22] S. Kase, Studies on melt spinning. IV. On the stability of melt spinning, J. Appl. Polym. Sci. **18**, 3279 (1974).
[23] Y. T. Shah and J. R. A. Pearson, On the stability of nonisothermal fiber spinning-general case, Ind. Eng. Chem. Fundam. **11**, 150 (1972).
[24] J. C. Chang, M. M. Denn, and F. T. Geyling, Effects of inertia, surface tension, and gravity on the stability of isothermal drawing of Newtonian fluids, Ind. Eng. Chem. Fundam. **20**, 147 (1981).
[25] B. P. Huynh and R. I. Tanner, Study of the non-isothermal glass fibre drawing process, Rheol. Acta **22**, 482 (1983).
[26] M. R. Myers, A model for unsteady analysis of preform drawing, AIChE J. **35**, 592 (1989).
[27] W. W. Schultz and S. H. Davis, One-dimensional liquid fibers, J. Rheol. **26**, 331 (1982).
[28] G. W. Scherer, Editorial comments on a paper by Gordon S. Fulcher, J. Am. Ceram. Soc. **75**, 1060 (1992).
[29] S. Kase and T. Matsuo, Studies on melt spinning. I. Fundamental equations on the dynamics of melt spinning, J. Polym. Sci. A **3**, 2541 (1965).
[30] G. K. Gupta, W. W. Schultz, E. M. Arruda, and X. Lu, Nonisothermal model of glass fiber drawing stability, Rheol. Acta **35**, 584 (1996).
[31] Q. Chouffart, Experimental and numerical investigation of the continuous glass fiber drawing process, Ph.D. thesis, Université de Liège, 2018.
[32] M. Taroni, C. J. W. Breward, L. J. Cummings, and I. M. Griffiths, Asymptotic solutions of glass temperature profiles during steady optical fibre drawing, J. Eng. Math. **80**, 1 (2013).
[33] D. He, J. J. Wylie, H. Huang, and R. M. Miura, Extension of a viscous thread with temperature-dependent viscosity and surface tension, J. Fluid Mech. **800**, 720 (2016).
[34] R. J. Fisher and M. M. Denn, Mechanics of nonisothermal polymer melt spinning, AIChE J. **23**, 23 (1977).
[35] F. Geyling and G. Homsy, Extensional instabilities of the glass fiber drawing process, Glass Technol. **21**, 95 (1980).
[36] J. Willien, Y. Demay, and J. Agassant, Stretching stability analysis of a Newtonian fluid: Application to Polyler spinning and glass drawing, J. Theor. Appl. Mech. **7**, 719 (1988).
[37] E. J. Doedel, A. R. Champneys, T. F. Fairgrieve, Y. A. Kuznetsov, B. Sandstede, and X. Wang, AUTO97 Continuation and bifurcation software for ordinary differential equations (1997), AUTO software is freely distributed on http://indy.cs.concordia.ca/auto/.
[38] M. Bechert, D. Schubert, and B. Scheid, Practical mapping of the draw resonance instability in film casting of Newtonian fluids, Eur. J. Mech. B **52**, 68 (2015).
[39] M. Bechert, D. W. Schubert, and B. Scheid, On the stabilizing effects of neck-in, gravity, and inertia in Newtonian film casting, Phys. Fluids **28**, 024109 (2016).
[40] W. W. Schultz and S. H. Davis, Effects of boundary conditions on the stability of slender viscous fibers, J. Appl. Mech. **51**, 1 (1984).
[41] M. Renardy, Draw resonance revisited, SIAM J. Appl. Math. **66**, 1261 (2006).
[42] J. R. A. Pearson, Y. T. Shah, and R. D. Mhaskar, On the stability of fiber spinning of freezing fluids, Ind. Eng. Chem. Fundam. **15**, 31 (1976).
[43] T. Matsumoto and D. C. Bogue, Draw resonance involving rheological transitions, Polym. Eng. Sci. **18**, 564 (1978).
[44] T. Hagen, On the effects of spinline cooling and surface tension in fiber spinning, J. Appl. Math. Mech./Z. Angew. Math. Mech. **82**, 545 (2002).